Composite Structures 304 (2023) 116392

Contents lists available at ScienceDirect

Composite Structures

journal homepage: www.elsevier.com/locate/compstruct

Damage behavior analysis of unidirectional fiber reinforced shape memory polymer composites

Zhengxian Liu [a], Tong Mu [b], Xin Lan [a,*], Liwu Liu [b], Wenfeng Bian [c], Yanju Liu [b], Jinsong Leng [a,*]

[a] Centre for Composite Materials and Structures, Harbin Institute of Technology (HIT), Harbin 150001, People's Republic of China
[b] Department of Astronautical Science and Mechanics, Harbin Institute of Technology (HIT), Harbin 150080, People's Republic of China
[c] Department of Civil Engineering, Harbin Institute of Technology (HIT), Weihai 264209, People's Republic of China

ARTICLE INFO

Keywords:
Shape memory polymer composites
Buckling deformation
Damage behavior

ABSTRACT

Shape memory polymer composites (SMPCs) are gradually being used in space deployable structures due to their unique shape memory properties and variable stiffness characteristics. Currently, the damage behavior of SMPC has not been systematically investigated, which affects its structural design and application. In this study, the damage behavior analysis of unidirectional fiber-reinforced SMPCs was investigated. The buckling deformation and damage modes of SMPC were analyzed theoretically. The strain energy of the matrix cracking and fiber fracture damage system was developed considering the compressive strain of the matrix. Additionally, the analytical expressions of the key parameters during bending were determined and the law of evolution was revealed. The damage mode analysis showed that decreasing fiber volume content and increasing thickness were more likely to result in matrix cracking damage. The fiber fracture would occur in the stretching region if the fiber volume content was less than a certain value. Finally, the experiment was performed to demonstrate the validity of the theoretical method. This work is significant for the design and optimization of the SMPC-based structure.

1. Introduction

Shape memory polymers (SMPs) are a kind of smart material that can realize the transformation between permanent shape and temporary shape upon exposure to an external stimulus such as thermal, magnetic field, electrical and light, etc [1–6]. When the external temperature is lower than the glass transition temperature (T_g), thermo-responsive SMPs are in the glassy state [7–9]. When the temperature rises above T_g, it transits into the rubbery state, and its modulus is hundreds of times lower than that of the glassy state [10–15]. It is worth noting that the mechanical properties such as modulus, strength, and recovery moment of SMPs can be greatly improved by introducing fibers [16–19]. For the unidirectional fiber-reinforced shape memory polymer composites (SMPCs), when the shear modulus of the matrix is not enough to resist the transverse deformation of the fiber during bending, the fiber will buckle [20,21].

Fiber-reinforced SMPCs can be applied as space deployable structures due to their excellent mechanical properties, light weight, high packing ratio and controllable deformation [22–24]. Some research has been conducted on the buckling deformation fiber-reinforced SMPCs. Campbell et al. [25,26] studied carbon fiber-reinforced shape memory epoxy, and observed the buckling deformation and damage mode by an electron microscope. Lan et al. [27,28] considered the strain energy in the compressing and non-buckling region and further studied the post-buckling behavior of SMPC. Some scholars also proposed a new micro-buckling solution to study the deformation of SMPC [29,30]. Xiong et al. [31] theoretically studied the in-plane and out-of-plane buckling of fiber, and found that in-plane buckling produces the lower energy needed for SMPC. Gall et al. [32] observed the fiber micro-buckling morphology of the fiber cloth-reinforced SMPC by a microscope, and found that fiber fracture and matrix cracking are the main damage modes. Previous research concentrated on the buckling deformation behavior of SMPC and did not theoretically analyze the damage mechanism and damage behavior. This research provides a theoretical foundation for SMPC-based design by in-depth investigation of the damage mechanism and damage behavior.

In this study, the damage behavior of unidirectional fiber-reinforced SMPC during bending was investigated. Firstly, the stress state analysis was used to determine damage modes under various parameters. Then, the strain energy and neutral surface position, critical buckling position,

* Corresponding authors.
E-mail addresses: lanxin@hit.edu.cn (X. Lan), lengjs@hit.edu.cn (J. Leng).

https://doi.org/10.1016/j.compstruct.2022.116392
Received 2 July 2022; Received in revised form 6 October 2022; Accepted 18 October 2022
Available online 22 October 2022

Table 1
Material parameters of the matrix and carbon fiber.

Material	Tensile modulus (MPa)	Shear modulus (MPa)	Poisson's ratio	Shear strength (MPa)	Tensile strength (MPa)
Matrix (T_g)	32	11	0.45	7.8	8.2
Fiber	45,000	–	0.3	–	1100

Table 2
Dimension parameters of SMPC.

Material	Thickness (mm)	Width (mm)	Length (mm)	Fiber volume content (%)	Fiber diameter (mm)
SMPC	2	5	30	20 or 8	0.008

critical damage position, half-wavelength, and amplitude of the matrix cracking damage and fiber fracture damage systems were developed considering the compressive strain of the matrix. Finally, a four-point bending test was used to validate the theoretical model.

2. Theoretical analysis

In this study, based on the micromechanics theory of composite materials, the ideal assumptions for damage analysis of unidirectional fiber-reinforced SMPC are as follows [33,34]:

- Each fiber is distributed evenly in the matrix. There is no interfacial separation between the fiber and the matrix during bending, and the fiber and matrix follow the equal strain assumption;
- When the fiber volume content is very low, the fiber is prone to tensile fracture in the stretching region. Since the elongation at break (T_g) of the matrix is much larger than that of the fiber, the load transferred to the matrix after the fiber breaks can be ignored. Therefore, it is assumed that the matrix will not degrade after fiber fracture;
- When surface matrix cracking occurs in the compressing and buckling region, the fiber will lose its load and break (as shown in Fig. 3), and the compressive bearing capacity of the broken part will be greatly reduced or even ignored. Therefore, it is assumed that the fiber will not bear the load alone after matrix cracking.

To provide a theoretical basis for the design and damage analysis of unidirectional fiber-reinforced SMPCs, a thermo-responsive shape memory epoxy (T_g = 150℃) was used as the matrix [22], which could achieve shape programming and shape recovery through temperature stimulation. The fiber selected in this study was a general low-modulus carbon fiber prepared by Guangwei Composite Materials Co., ltd. SMPC with low modulus and low fiber volume content was selected, allowing SMPC to achieve a high packaging ratio in engineering applications. The material parameters in Table 1 and the dimension parameters of SMPC in Table 2 would be adopted in the study unless otherwise specified.

2.1. Fiber buckling deformation and damage modes

Unidirectional fiber reinforced SMPC exhibits in-plane buckling when bending around a cylinder at T_g [27,28]. The buckling morphology of SMPC is shown in Fig. 1(a) and (b). Fig. 1(c) and (d) present detailed information about the deformation of fiber and matrix in the X-Y and Y-Z planes, respectively. When fiber buckling occurs, the cross-section of SMPC can be divided into three regions according to the stress state of the fiber: the compressing and buckling region (region I), the compressing and non-buckling region (region II) and the stretching region (region III) (as shown in Fig. 1(e)). z_{ns} and z_{cb} represent the neutral surface and critical fiber buckling positions, respectively.

The geometric shape of fiber buckling conforms to the sine/cosine wave rule, and the wave shape of the fiber can be given by the Eq. (1) [23].

$$y = A\cos\left(\frac{\pi x}{\lambda}\right) \tag{1}$$

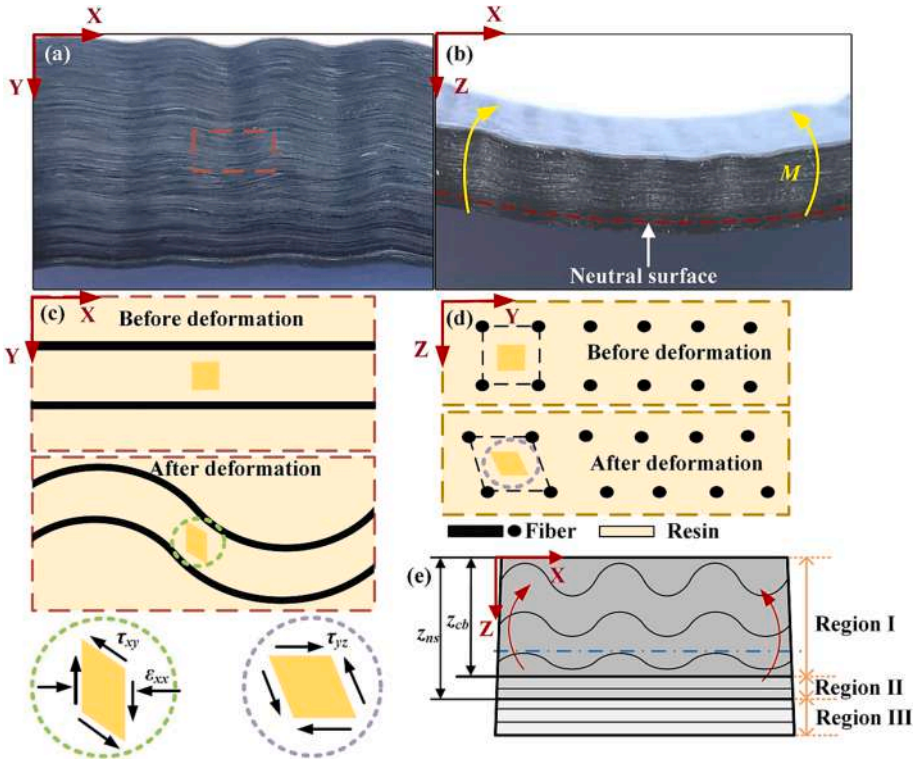

Fig. 1. Buckling deformation diagram of SMPC: (a) X-Y view; (b) X-Z view; (c) Detailed information on the deformation of fiber and matrix in the X-Y plane; (e) Detailed information on the deformation of fiber and matrix in the X-Z plane.

Where λ and A are the half-wavelength and amplitude of fiber buckling, respectively. The amplitude of fiber can be described as follows [23]:

$$A = \frac{2\lambda}{\pi}\sqrt{\kappa(z_{ns} - z)} \tag{2}$$

Where κ denotes the bending curvature. Substituting Eq. (2) into Eq. (1) yields the shape function of fiber buckling:

$$y = \frac{2\lambda}{\pi}\sqrt{\kappa(z_{ns} - z)}\cos\left(\frac{\pi x}{\lambda}\right) \tag{3}$$

Based on the equal strain assumption of the fiber and matrix, the shear stress of the matrix in the X-Y plane is given by:

$$\tau_{xy} = G_m\gamma_{xy} = \frac{G_m\delta y}{\delta x} = -2G_m\sqrt{\kappa(z_{ns} - z)}\sin\left(\frac{\pi x}{\lambda}\right) \tag{4}$$

Where G_m is the shear modulus of the matrix. When $z = 0$, $x = n\lambda/2$ ($n = 0,1,2\cdots\cdots$), the shear stress reaches the maximum. Because the amplitude of fiber buckling is different in the Z direction, there is shear deformation between two adjacent fibers in the Y-Z plane. The shear stress τ_{yz} can be expressed as follows:

$$\tau_{yz} = G_m\gamma_{yz} = G_m\frac{\delta y}{\delta z} = \frac{G_m\kappa\lambda}{\pi\sqrt{\kappa(z_{ns} - z)}}\cos\left(\frac{\pi x}{\lambda}\right) \tag{5}$$

The deformation modes of the fiber during bending can be divided into buckling, compression and tension. The curvature of the fiber in the buckling region can be described as follows:

$$\kappa_f = \frac{|y''|}{(1 + y'^2)^{\frac{3}{2}}} = \frac{|\frac{A\pi^2}{\lambda^2}\cos(\frac{\pi x}{\lambda})|}{[1 + \frac{A^2\pi^2}{\lambda^2}\sin^2(\frac{\pi x}{\lambda})]^{\frac{3}{2}}} \tag{6}$$

When $x = n\lambda$ and $z = 0$, the curvature of the fiber is the largest. At this time, the maximum buckling stress of the fiber can be expressed as follows:

$$\sigma_{f,max} = E_f\varepsilon_{f,max} = \frac{E_f dA\pi^2}{2\lambda^2} \tag{7}$$

Where E_f is the modulus of the fiber, and d is the diameter of the fiber. In the non-buckling region, the tensile/compressive stress of the fiber is:

$$\sigma_{fxx} = E_f\varepsilon_{xx} = E_f\kappa(z - z_{ns}) \tag{8}$$

When $z = t$ (t is the thickness), the tensile stress of the fiber reaches the maximum:

$$\sigma_{fxx,\max} = E_f\kappa(t - z_{ns}) \tag{9}$$

The neutral surface position (z_{ns}), critical buckling position (z_{cb}) and half-wavelength (λ) in the non-damaged state were derived in Lan's research [27].

$$z_{ns} = t - \frac{C}{\kappa}\left(\sqrt{1 + \frac{2\kappa t}{C}} - 1\right) \tag{10}$$

$$z_{cb} = z_{ns} - \frac{2C}{\kappa} \tag{11}$$

$$\lambda = \left[\frac{8\pi^3\nu_f E_f I_f\left(z_{ns}^2 - \frac{4C^2}{\kappa^2}\right)}{\nu_m G_m d^2\ln\left(\frac{z_{ns}\kappa}{2C}\right)}\right]^{\frac{1}{4}} \tag{12}$$

Where $C = \nu_m G_m/(\nu_m E_m + \nu_f E_f)$, ν_m and ν_f are the volume contents of matrix and fiber respectively, I_f is the moment of inertia of the fiber area. Previous studies [27,35] ignored the compressive strain of the matrix in the buckling region. To determine whether the compressive strain can be ignored in this study, the compressive strain and shear strain of the matrix during bending are compared. The ratio of shear strain to compressive strain is shown in Eqs. (13) and (14).

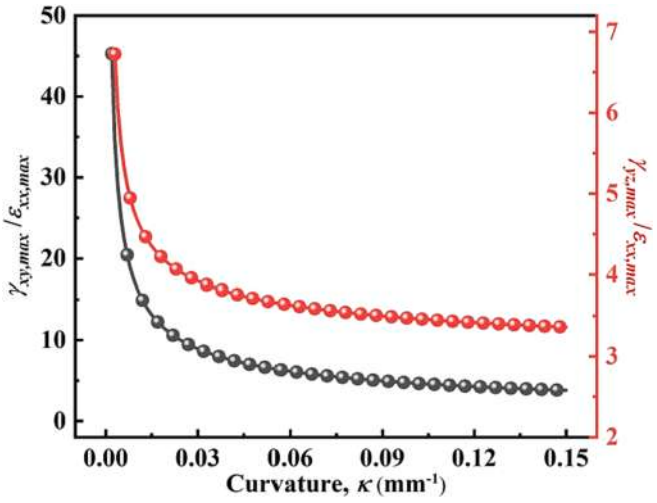

Fig. 2. Evolution of the ratio of shear strain to compressive strain during bending without considering the damage.

$$\frac{\gamma_{xy,\max}}{\varepsilon_{xx,\max}} = \frac{\sqrt{\kappa z_{ns}}}{2} \tag{13}$$

$$\frac{\gamma_{yz,\max}}{\varepsilon_{xx,\max}} = \frac{\lambda}{\pi z_{ns}\sqrt{2C}} \tag{14}$$

Fig. 2 displays the evolution of the ratio of shear strain to compressive strain during bending without considering damage. When the bending curvature is small, the compressive strain can be ignored due to the small compressive strain of the matrix. When the high packing ratio of SMPC is studied, the compressive strain of the matrix cannot be ignored.

By analyzing the matrix stress in the buckling region, the maximum stress appears at $z = 0$ or $z = z_{cb}$. At $z = 0$, the shear stress of the matrix can be given as Eq. (15). When x = $n\lambda/2$, the shear stress $\tau_{z=0}$ reaches the maximum (as shown in Eq. (16)).

$$\tau_{z=0} = \sqrt{\left(\frac{\sigma_{xx}}{2}\right)^2 + \tau_{xy}^2} = \sqrt{\frac{1}{4}(E_m\kappa z_{ns})^2 + 4G_m^2\kappa z_{ns}\sin^2\left(\frac{\pi x}{\lambda}\right)} \tag{15}$$

$$\tau_{z=0,\max} = \sqrt{\left(\frac{\sigma_{xx,\max}}{2}\right)^2 + \tau_{xy,\max}^2} = \sqrt{\frac{1}{4}E_m^2\kappa^2 z_{ns}^2 + 4G_m^2\kappa z_{ns}} \tag{16}$$

When $z = z_{cb}$, the shear stress of the matrix can be given as Eq. (17). When $\times = n\lambda$, the shear stress $\tau_{z=cb}$ reaches the maximum (as shown in Eq. (18)).

$$\tau_{z=z_{cb}} = \frac{G_m^2\kappa\lambda^2}{\pi^2(z_{ns} - z_{cb})}\cos^2\left(\frac{\pi x}{\lambda}\right) \tag{17}$$

$$\tau_{z=z_{cb},\max} = \frac{G_m\kappa\lambda}{\pi\sqrt{2C}} \tag{18}$$

According to the stress analysis of the fiber and matrix, there may be four damage modes: matrix cracking, delamination, fiber tensile fracture and fiber buckling fracture. The matrix cracking and delamination are caused by the matrix reaching its ultimate strength at $z = 0$ and $z = z_{cb}$, respectively. The fiber fracture is primarily caused by fibers attaining tensile strength at $z = 0$ or $z = t$. In this study, the maximum shear stress criterion was used to assess matrix cracking and delamination, and the maximum tensile stress criterion was used to assess fiber fracture. The damage mode of SMPC can be determined by comparing the stress states of the matrix and fiber at the dangerous position.

The influence of thickness and fiber volume content on the damage mode is shown in Fig. 3(a). There are three damage modes:

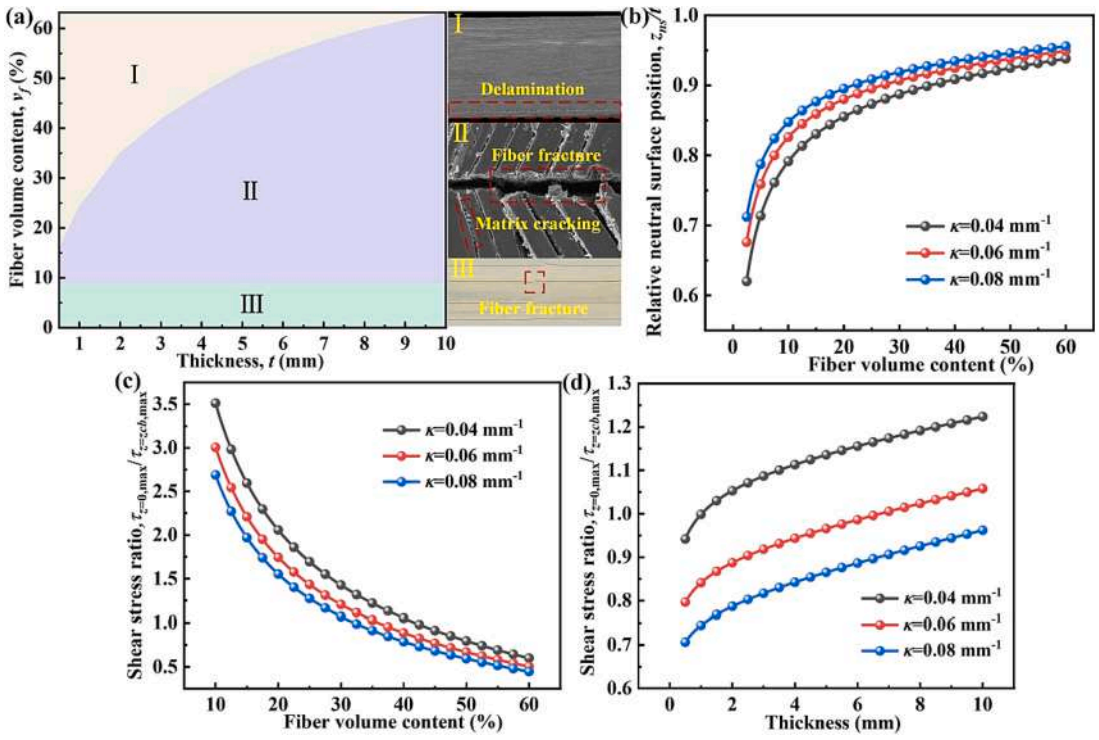

Fig. 3. (a) Influence of thickness and fiber volume content on damage mode (I: delamination damage mode; II: matrix cracking damage mode; III: fiber tensile fracture damage mode); (b) Variation of relative neutral surface position with fiber volume content; (c) Variation of shear stress ratios at $z = 0$ and $z = z_{cb}$ with fiber volume content; (d) Variation of shear stress ratios at $z = 0$ and $z = z_{cb}$ with thickness.

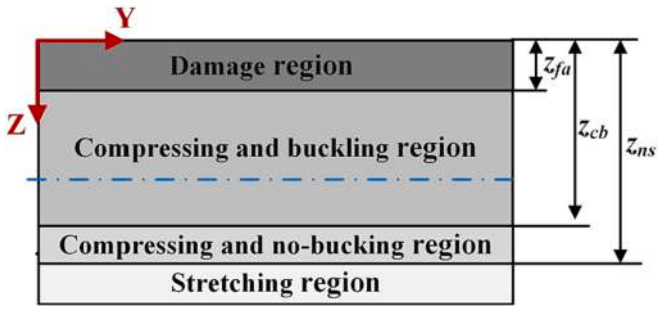

Fig. 4. Schematic diagram of the cross-section of the matrix cracking damage.

delamination, surface matrix cracking, and fiber tensile fracture. Notably, the distribution of damage modes in Fig. 3(a) is dependent on the data in Tables 1 and 2. When the fiber volume content is less than 8.57 %, the fiber tensile fracture damage will occur in the stretching region. This is due to the fact that as the fiber volume content decreases, the neutral surface position moves away from the stretching surface during bending, increasing the stress on the fiber in the stretching region (as shown in Fig. 3(b)). When the fiber volume content is above 8.57 %, the higher the fiber volume content is, the easier the delamination damage occurs. This is because as the fiber volume content increases, the shear stress ratio at $z = 0$ and $z = z_{cb}$ of the matrix gradually decreases, resulting in prone to delamination damage at $z = z_{cb}$ (as shown in Fig. 3 (c)). In the case of the same fiber volume content, the higher the thickness is, the easier the matrix cracks. This is because with the increase of thickness, the ratio of matrix shear stress at $z = 0$ and $z = z_{cb}$ increases, resulting in more prone to matrix cracking at $z = 0$ (as shown in Fig. 3(d)). At the same time, when the surface matrix cracking occurs, the fiber buckling fracture will occur at the peak or trough of the fiber buckling. This is because the buckled fiber loses the load of the matrix.

2.2. Strain energy of matrix cracking damage system

According to the damage mode analysis, when the fiber volume content is 20 %, matrix cracking damage will occur during bending. When the shear stress of the matrix in the buckling region exceeds the shear strength, matrix cracking damage will occur at $z = 0$. According to the stress state of the fiber, the cross-section can be divided into four regions: damage region, compressing and buckling region, compressing and non-buckling region and stretching region (as shown in Fig. 4). z_{fa} represents the critical damage position.

The shape memory resin (T_g) and fiber adopted in this study can be regarded as linear elastic materials [27], so the total strain energy of the system is given by:

$$U_T = \frac{1}{2}\int \varepsilon_{ij}\sigma_{ij}dv = \frac{1}{2}\int \left(\varepsilon_{xx}\sigma_{xx} + \varepsilon_{yy}\sigma_{yy} + \varepsilon_{zz}\sigma_{zz} + \tau_{xy}\gamma_{xy} + \tau_{yz}\gamma_{yz} + \tau_{xz}\gamma_{xz}\right)dv \tag{19}$$

According to the buckling deformation analysis of SMPC, the strain energy of the matrix cracking damage system is given as follows:

$$U_T^m = U_{xx}^m + U_{xy}^m + U_{yz}^m + U_{fb}^m + U_{mxx}^m \tag{20}$$

Where *Um T* denotes the total strain energy of the matrix damage system; *Um xx* denotes the strain energy in the non-buckling region; *Um xy* and *Um xz* denote the strain energy caused by the shear strain γ_{xy} and γ_{xz}, respectively; *Um fb* denotes the strain energy of buckling fiber; *Um mxx* denotes the compressive strain energy of the matrix in the buckling region. The strain energy in the non-buckling region of the matrix damage system can be represented as follows:

$$\begin{aligned} U_{xx}^m &= \frac{1}{2}\int_{z_{cb}}^{t}\int_0^b\int_0^l E\varepsilon_{xx}^2 dxdydz \\ &= \frac{blE\kappa^2}{6}\left[(t - z_{ns})^3 + (z_{ns} - z_{cb})^3\right] \end{aligned} \tag{21}$$

Where $E = \nu_f E_f + \nu_m E_m$, b and l represent the width and length of

SMPC, respectively. The strain energy caused by the shear strain γ_{xy} of the matrix cracking damage system is:

$$U_{xy}^{m} = \frac{1}{2}\int_{z_{fa}}^{z_{cb}}\int_{0}^{b}\int_{0}^{l}\nu_m G_m \gamma_{xy}^2 dxdydz = \frac{bl\nu_m G_m \kappa}{2}\left[\left(z_{ns}-z_{fa}\right)^2-\left(z_{ns}-z_{cb}\right)^2\right] \tag{22}$$

The strain energy caused by the shear strain γ_{yz} can be calculated as follows:

$$U_{yz}^{m} = \frac{1}{2}\int_{z_{fa}}^{z_{cb}}\int_{0}^{l}\int_{0}^{b}\nu_m G_m \gamma_{yz}^2 dxdydz = \frac{bl\nu_m G_m \lambda^2 \kappa}{4\pi^2}\ln\left(\frac{z_{ns}-z_{fa}}{z_{ns}-z_{cb}}\right) \tag{23}$$

The strain energy of fiber buckling can be given by:

$$U_{fb}^{m} = \frac{1}{2}\int_{z_{fa}}^{z_{cb}}\frac{b}{h^2}\nu_f E_f I_f \int_{0}^{l}\left(\frac{d^2y}{dx^2}\right)dxdz = \frac{2bl\pi^2\nu_f E_f I_f \kappa}{d^2\lambda^2}\left[\left(z_{ns}-z_{fa}\right)^2-\left(z_{ns}-z_{cb}\right)^2\right] \tag{24}$$

Where h represents the distance between adjacent fibers. The compressive strain energy of the matrix in the buckling region can be expressed as follows:

$$U_{mxx}^{m} = \frac{1}{2}\int_{z_{fa}}^{z_{cb}}\int_{0}^{b}\int_{0}^{l}\nu_m E_m \varepsilon_{xx}^2 dxdydz = \frac{bl\nu_m E_m \kappa^2}{6}\left[\left(z_{ns}-z_{fa}\right)^3-\left(z_{ns}-z_{cb}\right)^3\right] \tag{25}$$

Substituting Eqs. (21)-(25) into Eq. (20) gives the total strain energy of the matrix cracking damage system:

$$U_T^m = \frac{blE\kappa^2}{6}\left[\left(t-z_{ns}\right)^3+\left(z_{ns}-z_{cb}\right)^3\right]+\frac{bl\nu_m E_m \kappa^2}{6}\left[\left(z_{ns}-z_{fa}\right)^3-\left(z_{ns}-z_{cb}\right)^3\right] +\frac{bl\nu_m G_m \kappa}{2}\left[\left(z_{ns}-z_{fa}\right)^2-\left(z_{ns}-z_{cb}\right)^2\right]+\frac{bl\nu_m G_m \lambda^2\kappa}{4\pi^2}\ln\left(\frac{z_{ns}-z_{fa}}{z_{ns}-z_{cb}}\right) +\frac{2bl\pi\nu_f E_f I_f \kappa}{d^2\lambda^2}\left[\left(z_{ns}-z_{fa}\right)^2-\left(z_{ns}-z_{cb}\right)^2\right] \tag{26}$$

When $z_{fa} = 0$, we can obtain the strain energy of the non-damage system:

$$U_T = \frac{blE\kappa^2}{6}\left[\left(t-z_{ns}\right)^3+\left(z_{ns}-z_{cb}\right)^3\right]+\frac{bl\nu_m E_m \kappa^2}{6}\left[z_{ns}^3+\left(z_{ns}-z_{cb}\right)^3\right] +\frac{bl\nu_m G_m \kappa}{2}z_{cb}\left(2z_{ns}-z_{cb}\right)+\frac{bl\nu_m G_m \lambda^2\kappa}{4\pi^2}\ln\left(\frac{z_{ns}}{z_{ns}-z_{cb}}\right) +\frac{2\pi bl\nu_f E_f I_f \kappa}{\lambda^2 d^2}z_{cb}\left(2z_{ns}-z_{cb}\right) \tag{27}$$

When $\kappa = \kappa_0$ ($\kappa_0 > \kappa_{fc}$), SMPC is bent again after shape recovery. In this case, the positions of the neutral surface, critical buckling and critical damage can be expressed as z_{fa0}, z_{ns0} and z_{cb0}, respectively. Hence, the strain energy of the system with damage can be described as follows:

$$U_{T0}^m = \frac{blE\kappa^2}{6}\left[\left(t-z_{ns0}\right)^3+\left(z_{ns0}-z_{cb0}\right)^3\right]+\frac{bl\nu_m E_m \kappa^2}{6}\left[\left(z_{ns0}-z_{fa0}\right)^3-\left(z_{ns0}-z_{cb0}\right)^3\right] +\frac{bl\nu_m G_m \kappa}{2}\left[\left(z_{ns0}-z_{fa0}\right)^2-\left(z_{ns0}-z_{cb0}\right)^2\right]+\frac{bl\nu_m G_m \lambda^2\kappa}{4\pi^2}\ln\left(\frac{z_{ns0}-z_{fa0}}{z_{ns0}-z_{cb0}}\right) +\frac{2bl\pi\nu_f E_f I_f \kappa}{d^2\lambda^2}\left[\left(z_{ns0}-z_{fa0}\right)^2-\left(z_{ns0}-z_{cb0}\right)^2\right] \tag{28}$$

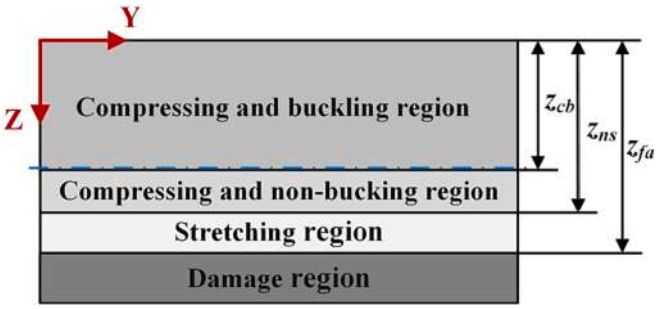

Fig. 5. Schematic diagram of the cross-section of the fiber fracture damage system.

2.3. Strain energy of fiber fracture tensile damage system

When the fiber volume content is less than 8.57 %, the fiber tensile fracture damage is prone to occur during bending (as shown in Fig. 3). The fiber fracture will begin from the stretching region at this point. The schematic diagram of the cross-section of the fiber fracture damage system is shown in Fig. 5.

According to the buckling deformation analysis of SMPC, we get the strain energy of the fiber fracture damage system:

$$U_T^f = U_{xx}^f + U_{xy}^f + U_{yz}^f + U_{fb}^f + U_{mxx}^f + U_{fmxx}^f \tag{29}$$

Where *Uf T* denotes the total strain energy of the fiber damage system; *Uf xx* denotes the strain energy in the non-buckling region; *Uf xy* and *Uf xz* denote the strain energy caused by the shear strain γ_{xy} and γ_{xz}, respectively; *Uf fb* denotes the strain energy of fiber buckling; *Uf mxx* and *Uf fmxx* denote the compressive strain energy of the matrix in the buckling and damage regions, respectively.

The strain energy in the non-buckling region of the fiber fracture damage system can be evaluated as follows:

$$U_{xx}^f = \frac{1}{2}\int_{z_{cb}}^{z_{fa}}\int_{0}^{b}\int_{0}^{l}E\varepsilon_x^2 dxdydz = \frac{blE\kappa^2}{6}\left[\left(z_{fa}-z_{ns}\right)^3+\left(z_{ns}-z_{cb}\right)^3\right] \tag{30}$$

The strain energy caused by the shear strain γ_{xy} of the fiber damage system can be calculated as follows:

$$U_{xy}^f = \frac{1}{2}\int_{0}^{z_{cb}}\int_{0}^{b}\int_{0}^{l}\nu_m G_m \gamma_{xy}^2 dxdydz = \frac{bl\nu_m G_m \kappa}{2}\left[z_{ns}^2-\left(z_{ns}-z_{cb}\right)^2\right] \tag{31}$$

The strain energy caused by the shear strain γ_{yz} of the fiber damage system is obtained as follows:

$$U_{yz}^f = \frac{1}{2}\int_{0}^{zcb}\int_{0}^{l}\int_{0}^{b}\nu_m G_m \gamma_{yz}^2 dxdydz = \frac{bl\nu_m G_m \lambda^2\kappa}{4\pi^2}\ln\left(\frac{z_{ns}}{z_{ns}-z_{cb}}\right) \tag{32}$$

The strain energy of fiber buckling in the fiber damage system is calculated as follows:

$$U_{fb}^f = \frac{1}{2}\int_{0}^{z_{cb}}\frac{b}{h^2}E_f I_f \int_{0}^{l}\left(\frac{d^2y}{dx^2}\right)dxdz = \frac{2bl\pi^2 E_f I_f \kappa}{d^2\lambda^2}\left[z_{ns}^2-\left(z_{ns}-z_{cb}\right)^2\right] \tag{33}$$

The compressive strain energy of the matrix in the buckling region of the fiber damage system is:

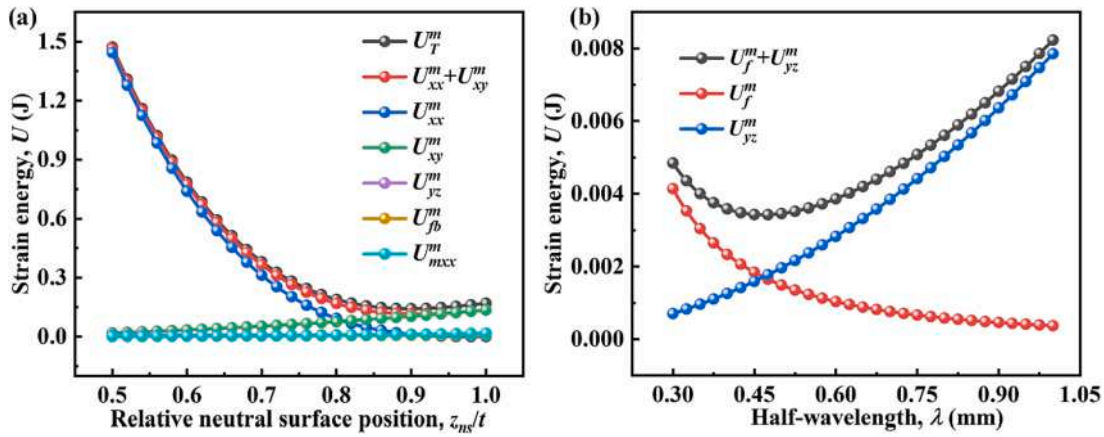

Fig. 6. (a) Relationship between the strain energy and the neutral surface position ($\lambda = 0.7$, κ=0.07 mm^{-1}, $z_{fa} = 0.4$ mm); (b) Relationship between strain energy and half-wavelength (κ=0.07 mm^{-1}).

$$U_{mxx}^f = \frac{1}{2}\int_0^{z_{cb}}\int_0^b\int_0^l v_m E_m \varepsilon_x^2 dxdydz = \frac{blv_m E_m \kappa^2}{6}\left[z_{ns}^3 - (z_{ns}-z_{cb})^3\right] \tag{34}$$

The tensile strain energy of the matrix in the damaged region is given as follows:

$$U_{fmxx}^f = \frac{1}{2}\int_{z_{fa}}^t\int_0^b\int_0^l v_m E_m \varepsilon_x^2 dxdydz = \frac{blv_m E_m \kappa^2}{6}\left[(t-z_{ns})^3 - (z_{fa}-z_{ns})^3\right] \tag{35}$$

Substituting Eqs. (30)-(35) into Eq. (29) gives the total strain energy of the fiber fracture damage system:

$$\begin{aligned} U_{Tf}^f = {} & \frac{blE\kappa^2}{6}\left[(z_{fa}-z_{ns})^3 + (z_{ns}-z_{cb})^3\right] + \frac{blv_m E_m\kappa^2}{6}\left[(t-z_{ns})^3 - (z_{fa}-z_{ns})^3\right] \\ & + \frac{blv_m E_m\kappa^2}{6}\left[z_{ns}^3 - (z_{ns}-z_{cb})^3\right] + \frac{blv_m G_m\kappa}{2}\left[z_{ns}^2 - (z_{ns}-z_{cb})^2\right] \\ & + \frac{blv_m G_m\lambda^2\kappa}{4\pi^2}\ln\left(\frac{z_{ns}}{z_{ns}-z_{cb}}\right) + \frac{2bl\pi^2 v_f E_f I_f \kappa}{d^2\lambda^2}\left[z_{ns}^2 - (z_{ns}-z_{cb})^2\right] \end{aligned} \tag{36}$$

When $\kappa = \kappa_0$ ($\kappa_0 > \kappa_{fc}$), SMPC is bent again after shape recovery. At this point, the strain energy of the system with damage can be obtained as the same as that of the matrix fracture system.

3. Key parameters analysis

3.1. Key parameters of the matrix cracking damage system

When matrix cracking occurs, the shear stress of the matrix first reaches the shear strength at $z = 0$. The following equation can be obtained:

$$\tau_{z=0,\max} = \sqrt{\frac{1}{4}E_m^2\kappa^2 z_{ns}^2 + 4G_m^2\kappa z_{ns}} = \tau_s \tag{37}$$

Where τ_s is the shear strength of the matrix. The critical curvature of the matrix cracking can be determined as:

$$\kappa_{fc} = \frac{a+\sqrt{2aC}}{t} \tag{38}$$

Where$a = \frac{-8G_m^2+2\sqrt{16G_m^4+E_m^2\tau_s^2}}{E_m^2}$. The relationship between z_{ns} and z_{fa} is given as follows:

$$\kappa(z_{ns}-z_{fa}) = a \tag{39}$$

The compressing and non-buckling region is very small [27]. When the compressing and non-buckling region is ignored, the strain energy can be approximated as Eq. (40). The relationship between the strain energy and z_{ns}/t is shown in Fig. 6(a). It can be noted that *Um xx* and *Um xy* are much larger than other strain energies. Therefore, when solving z_{ns} and z_{cb}, the strain energy can be simplified to Eq. (41). At the same time, *Um xx* + *Um xy* has minimum energy, so z_{fa}, z_{ns} and z_{cb} can be derived by the minimum energy principle and combining Eq. (39) (as shown in Eq. (42)).

$$\begin{aligned} U_T^m = {} & \frac{blE\kappa^2}{6}(t-z_{ns})^3 + \frac{blv_m G_m\kappa}{2}(z_{ns}-z_{fa})^2 + \frac{blv_m E_m\kappa^2}{6}(z_{ns}-z_{fa})^3 \\ & + \frac{blv_m G_m\lambda^2\kappa}{4\pi^2}\ln\left[\frac{4(z_{ns}-z_{fa})\sqrt{v_f}}{d\sqrt{\pi}}\right] + \frac{2bl\pi v_f E_f I_f\kappa}{\lambda^2 d^2}(z_{ns}-z_{fa})^2 \end{aligned} \tag{40}$$

$$\widehat{U}_{Tf-r}(z_{cb},z_{ns}) = U_{xx-r} + U_{xy-r} \tag{41}$$

$$\begin{cases} \dfrac{\partial\widehat{U}(z_{cb},z_{ns})}{\partial z_{cb}} = 0 \\ \dfrac{\partial\widehat{U}(z_{cb},z_{ns})}{\partial z_{ns}} = 0 \end{cases} \tag{42}$$

Combining Eq. (39) and Eq. (42), we obtain the following results:

$$z_{ns} = t - \frac{\sqrt{2aC}}{\kappa} \tag{43}$$

$$z_{cb} = t - \frac{2C+\sqrt{2aC}}{\kappa} \tag{44}$$

$$z_{fa} = t - \frac{a+\sqrt{2aC}}{\kappa} \tag{45}$$

According to Eq. (26), only *Um yz* and *Um f* are related to half-wavelength. The relationship between strain energy and half-wavelength of the matrix damage system is shown in Fig. 6(b). As the half-wavelength changes, the strain energy has a minimum. Therefore, the half-wavelength can be derived by the minimum energy principle (as shown in Eq. (46)).

$$\lambda = \left[\frac{8\pi^3 v_f E_f I_f\left(a^2-4C^2\right)}{d^2\nu_m G_m\kappa^2\ln\left(\frac{2a^2}{C}\right)}\right]^{\frac{1}{4}} \tag{46}$$

Inserting Eq. (46) into Eq. (2), the amplitude of the fiber can be obtained. When the bending curvature reaches κ_0 ($\kappa_0 > \kappa_{fc}$), the critical damage position reaches z_{fa0} at this time. SMPC is bent again after shape

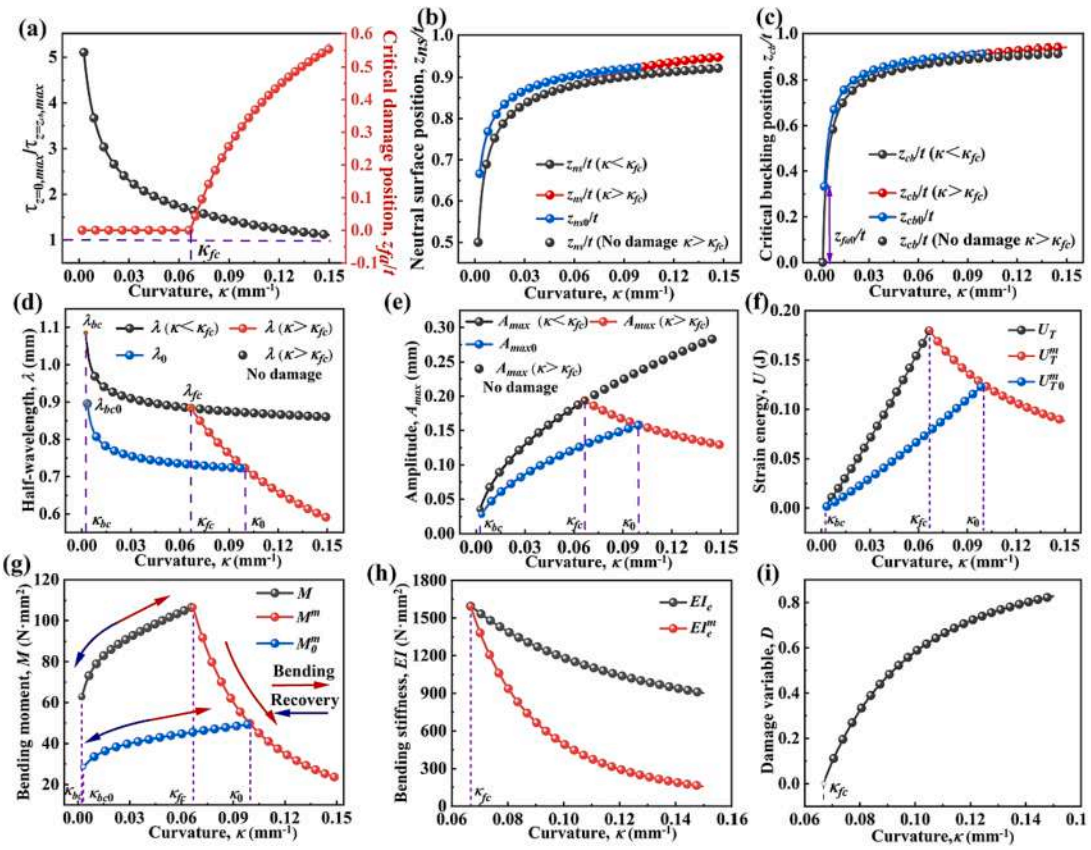

Fig. 7. Evolution of the matrix cracking damage system during bending: (a) $\tau_{z=0,\max}/\tau_{z=cb,\max}$-$\kappa$ and $z_{fa\text{-}r}/t$-κ; (a) z_{cb}/t-κ; (b) z_{ns}/t-κ; (d) λ-κ; (e) λ-κ; (f)A-κ; (f)U-κ; (g)M-κ; (h)EI-κ; (i)D-κ.

recovery. The relationship between the critical damage position z_{fa0} and the curvature κ_0 can be described as follows:

$$z_{fa0} = t - \frac{\sqrt{2aC} + a}{\kappa_0} \tag{47}$$

The neutral surface position and critical buckling position of the rebending system can be obtained by the minimum energy principle (as shown in Eqs. (48) and (49)).

$$z_{ns0} = t - \frac{C}{\kappa}\left(\sqrt{1 + \frac{2\kappa(a + \sqrt{2aC})}{C\kappa_0}} - 1\right) \tag{48}$$

$$z_{cb0} = z_{ns0} - \frac{2C}{\kappa} \tag{49}$$

When $z_{cb0} = z_{fa0}$, the critical buckling of the fiber occurs in the damaged state, and the critical buckling curvature can be obtained as follows:

$$\kappa_{bc0} = \frac{4C}{t - z_{fa0}} \tag{50}$$

The strain energy of the rebending system with matrix cracking damage can be obtained by substituting Eqs. (47)-(49) into Eq. (28). At this time, the half-wavelength and amplitude of the rebending system can be expressed by the minimum energy principle.

The bending moment and equivalent bending stiffness can be given as Eqs. (51) and (52).

$$M^m = \left.\frac{\partial U_{T0}}{l\partial\kappa}\right|_{\kappa=\kappa_0^-} \tag{51}$$

$$EI_e^m = \frac{M^m}{l\kappa_0} \tag{52}$$

The bending stiffness variation is used to describe the damage variable in the study. The damage variable (D) can be obtained as follows:

$$D = 1 - \frac{EI_e^m}{EI_e} = 1 - \left(\left.\frac{\partial U_{T0}}{\kappa_0\partial\kappa}\right|_{\kappa=\kappa_0^-}\right) \Big/ \left(\frac{\partial U_T}{\kappa\partial\kappa}\right) \tag{53}$$

3.2. Key parameters of the fiber tensile fracture damage system

In this study, the fiber fracture damage behavior of SMPC with 8 % fiber volume content was investigated. When the fiber stress reaches the tensile strength, the following equation can be obtained.

$$\sigma_f = E_f\kappa(t - z_{ns}) = \sigma_{sf} \tag{54}$$

Where σ_{sf} is the tensile strength of the fiber. The critical curvature of the fiber fracture damage can be derived as follows:

$$\kappa_{fc} = \frac{\sigma_s^2 + 2\sigma_{sf}E_fC}{2E_f^2Ct} \tag{55}$$

The relationship between z_{ns} and z_{fa} can be described as follows:

$$\kappa\left(z_{fa} - z_{ns}\right) = \sigma_{sf}/E_f \tag{56}$$

When ignoring the compressing and non-buckling region, the calculation method of fiber fracture damage system is consistent with that of the matrix fracture damage system. The expressions of neutral surface position, critical buckling position, critical damage position, and half-wavelength of fiber fracture damage system can be derived by the minimum energy principle.

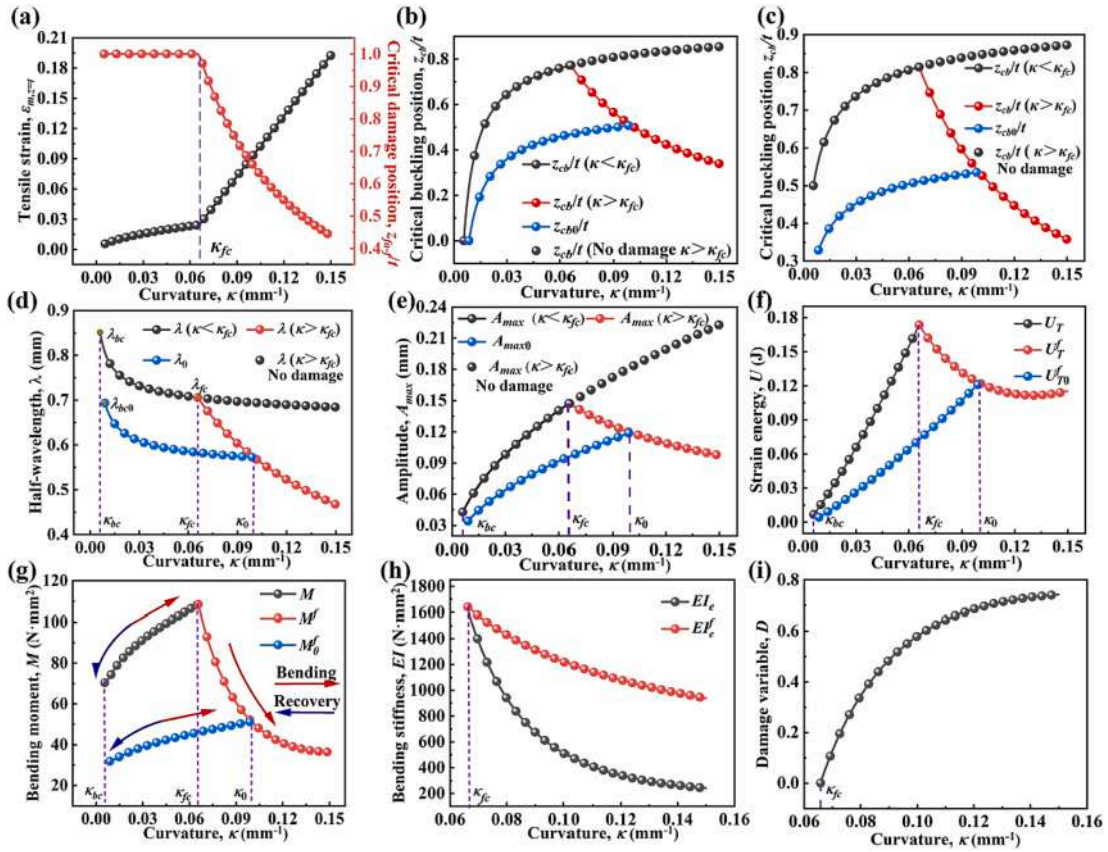

Fig. 8. Evolution of the fiber fracture damage system during bending: (a) $\tau_{z=0,\max}/\tau_{z=cb,\max}$-$\kappa$ and $z_{fa\text{-}r}/t$-κ; (a) z_{cb}/t-κ; (b) z_{ns}/t-κ; (d) λ-κ; (e) λ-κ; (f)A-κ; (f)U-κ; (g)M-κ; (h)EI-κ; (i)D-κ.

$$z_{ns} = \frac{\sigma_s^2}{2CE_f^2\kappa} \tag{57}$$

$$z_{cb} = z_{ns} - \frac{2C}{\kappa} \tag{58}$$

$$z_{fa} = z_{ns} + \frac{\sigma_s}{E_f\kappa} \tag{59}$$

$$\lambda = \left[\frac{8\pi^3\nu_f E_f I_f\left(z_{ns}^2 - \frac{4C^2}{\kappa^2}\right)}{\nu_m G_m d^2 \ln\left(\frac{z_{ns}\kappa}{2C}\right)}\right]^{\frac{1}{4}} \tag{60}$$

Substituting Eq. (2) into Eq (60), the amplitude of the fiber damage system can be obtained. When the bending curvature reaches κ_0 ($\kappa_0 > \kappa_{fc}$), the critical damage position reaches z_{fa0}. At this time, SMPC is bent again after shape recovery. The relationship between the z_{fa0} and κ_0 can be described as follows:

$$z_{fa0} = \frac{\sigma_s^2 + 2CE_f\sigma_s}{2CE_f^2\kappa_0} \tag{61}$$

The neutral surface position and critical buckling position of the rebending system can be determined by the minimum energy principle (as shown in Eqs (62) and (63)). Similarly, the half-wavelength and amplitude of the rebending system can be obtained.

$$z_{ns0} = z_{fa0} - \frac{C}{\kappa}\left(\sqrt{1 + \frac{2\kappa z_{fa0}}{C}} - 1\right) \tag{62}$$

$$z_{cb0} = z_{ns0} - \frac{2C}{\kappa} \tag{63}$$

4. Results and analysis

4.1. Matrix cracking damage behavior

Fig. 7 illustrates the evolution of the fiber fracture damage system during bending ($V_f = 20$ %). The evolution of $\tau_{z=0,\max}/\tau_{z=cb,\max}$ and z_{fa}/t of the matrix cracking damage system during bending is shown in Fig. 7 (a). When κ less than 0.15, the shear stress ratio $\tau_{z=0,\max}/\tau_{z=zcb,\max}$ is greater than 1, which means that only the matrix cracking damage will occur during bending. The critical damage position increases gradually after the damage occurs. Fig. 7 (b) and (c) display the evolution of the z_{ns}/t and z_{cb}/t during bending. As the curvature increases, z_{ns} and z_{cb} gradually approach the outside of the stretch. When $\kappa > \kappa_{fc}$, the change rate of z_{ns}/t and z_{cb}/t is further accelerated due to matrix cracking.

The evolution of half-wavelength and amplitude during bending is shown in Fig. 7(d) and (e). When the fiber buckling occurs, the half-wavelength jumps from infinity to 1.08 mm. If the SMPC is not damaged, the half-wavelength gradually stabilizes, and the increase rate of amplitude slows down with the increase of bending curvature. When $\kappa > \kappa_{fc}$, as the matrix cracking grows, the amplitude and half-wavelength at the critical buckling position are gradually reduced. Fig. 7(f) and (g) illustrate the evolution of strain energy and bending moment. When $\kappa < \kappa_{fc}$, the strain energy and bending moment gradually raise with the increase of bending curvature. When $\kappa > \kappa_{fc}$, with the increase of bending curvature, the matrix cracking propagation leads to the decrease of strain energy and bending moment. The evolution of equivalent bending stiffness and damage variable is shown in Fig. 7(h) and (i). In the undamaged state, the equivalent bending stiffness of SMPC decreases due to fiber buckling. When the matrix cracking occurs, the equivalent bending stiffness further reduces. At the same time, the rising rate of damage variable gradually slows down.

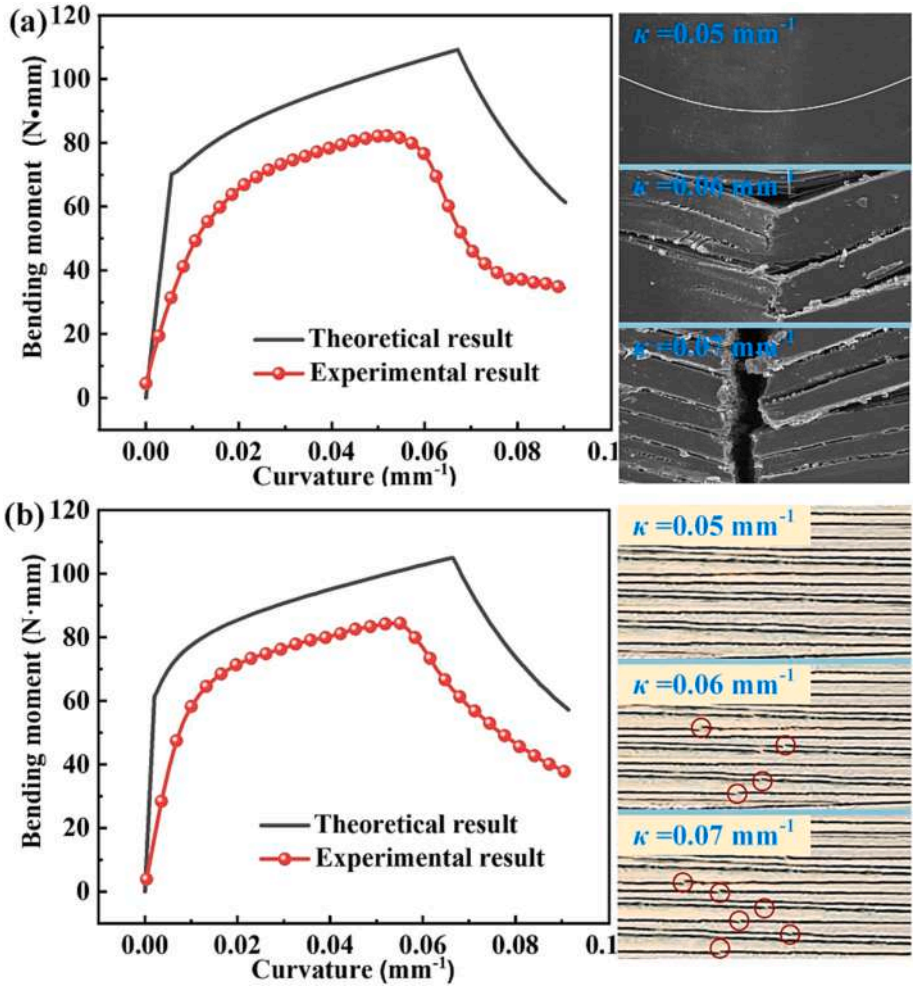

Fig. 9. Comparison of moment–curvature curves between the theoretical model and the experimental test.

4.2. Fiber tensile fracture damage behavior

Fig. 8 illustrates the evolution of the fiber fracture damage system during bending ($V_f = 8$ %). When the fiber volume content is 8 %, only fiber tensile fracture damage will occur. The evolution of $\varepsilon_{m,z=t}$ and z_{fa}/t during bending is illustrated in Fig. 8(a). $\varepsilon_{m,z=t}$ represents the tensile strain of the matrix at $z = t$. As the bending moment increases, the z_{fa} gradually approaches the compressed surface, and the tensile strain $\varepsilon_{m,z=t}$ is almost linearly increased. Since the elongation at break of the matrix at T_g was very high, the matrix cracking damage was not considered in this study. Fig. 8(b) and (c) plot the z_{cb}/t and z_{ns}/t values during bending, respectively. Different from the matrix cracking damage, z_{cb}/t and z_{ns}/t suddenly drop when $\kappa > \kappa_{fc}$. This is due to the stiffness reduction caused by fiber fracture in the stretching region.

Fig. 8(d) and (e) show the evolution of the half-wavelength and amplitude, respectively. The half-wavelengths of critical buckling and critical damage are 0.85 mm and 0.7 mm, respectively. It can be noted that the changing trend of the half-wavelength and amplitude of the fiber fracture damage is consistent with that of the matrix cracking damage. Fig. 8(f) and (g) display the evolution of strain energy and bending moment, respectively. In contrast to matrix cracking, when $\kappa > \kappa_{fc}$, as the bending curvature increases, the strain energy first decreases and then increases, and the rate of variation of bending moment decreases gradually. This is because the fiber fracture does not cause the matrix cracking. When the bending curvature reaches a certain value, the strain energy begins to increase. The evolution of the equivalent bending stiffness and damage variable during bending is shown in Fig. 8 (h) and (i). Similar to matrix cracking damage, the equivalent bending stiffness drops to varying degrees with increasing bending curvature due to the increase of fiber buckling and damage. The changing trend of the damage variable of the fiber fracture damage system was generally consistent with that of the matrix cracking damage system.

5. Experimental verification

Four-point bending tests on unidirectional fiber-reinforced SMPC at 150 °C were performed to validate the theoretical model. The testing specimen's dimensions were 200 mm × 5 mm × 2 mm. The fiber volume content was 22 % and 8 % respectively, which corresponded to the matrix cracking and delamination damage respectively. The prepreg method was used to manufacture SMPC. In particular, the thickness of SMPC was controlled by placing a 2 mm hard silicone strip around the unidirectional fiber prepreg, and then the fiber volume content was controlled by balancing the proportions of fiber prepreg and shape memory epoxy film. We chose a support span of 50 mm, a loading span of 25 mm, and a loading rate of 2 mm/min to investigate the high folding ratio of SMPC during the test. The maximum deformation deflection during the loading process was 53 mm.

Fig. 9 compares of the moment–curvature curves of the theoretical model and the experimental test. The results show that the trend of the theoretical model prediction is generally consistent with that of the experimental test curve. However, the theoretical prediction curve is higher than the experimental curve before damage occurs. The main reason is that the theoretical model is based on the equal strain

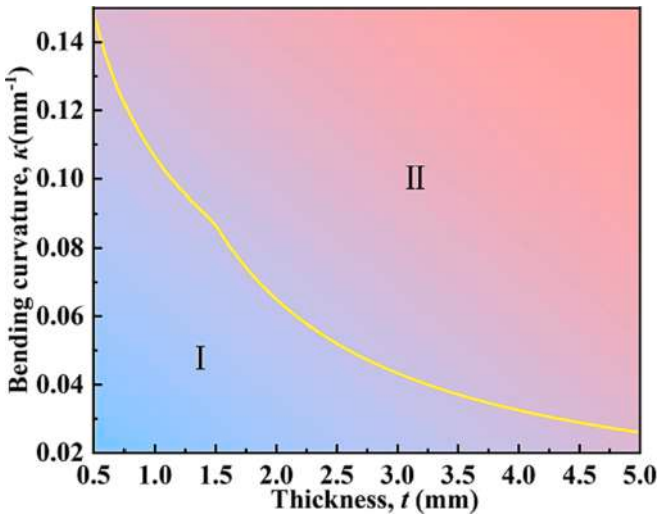

Fig. 10. Relationship curve between thickness and bending curvature in the structural design: I represents the safety allowable region; II represents the dangerous region.

assumption of the fiber and matrix. However, the combination of fiber and matrix may not be ideal in the actual material manufacturing process, resulting in the critical damage curvature in the experiment being greater than that in the theory. At the same time, the fiber and matrix in the theoretical model are based on the equal strength assumption, so the load change suddenly after damage, but it is a smooth transition in the experiment.

6. Applications in structural design

The space deployable structure based on SMPCs has the advantages of lightweight simple, controllable deployment and low impact. The damage mechanism and damage behavior of SMPC are systematically discussed in this study, which provides a theoretical foundation for structural design. When designing the size parameters, the thickness and bending radius of the SMPC structure should be considered. Taking the fiber volume content of 30 % as an example, the structural dimensions of SMPC were designed by using the material parameters in Table 1. By comparing Eqs. (7), (9), (16) and (18) with the strength of matrix and fiber, the relationship curve between thickness and bending curvature in design can be obtained (as shown in Fig. 10). Region I is the safety allowable area in the design. When the structural thickness and bending radius are below the curve, damage can be effectively avoided. It is worth noting that the SMPC-based lenticular tube was designed according to the theoretical analysis in this study, and the flexible solar array system based on the lenticular tube was successfully deployed in orbit for the first time in the world (as shown in Fig. 11) [36].

7. Conclusions

In this study, the damage behavior of unidirectional fiber-reinforced SMPC was investigated. The influence of fiber volume content and thickness on the damage mode was obtained through the deformation analysis of fiber buckling. The results revealed that increasing fiber volume content and decreasing fiber thickness are more likely to cause delamination damage at the critical buckling position. Conversely, it was easier to cause matrix cracking damage, but when the fiber volume content fell below a certain value, only fiber tensile fracture damage mode occurred. Considering the compressive strain of the matrix, the strain energy of matrix cracking and fiber fracture damage systems was

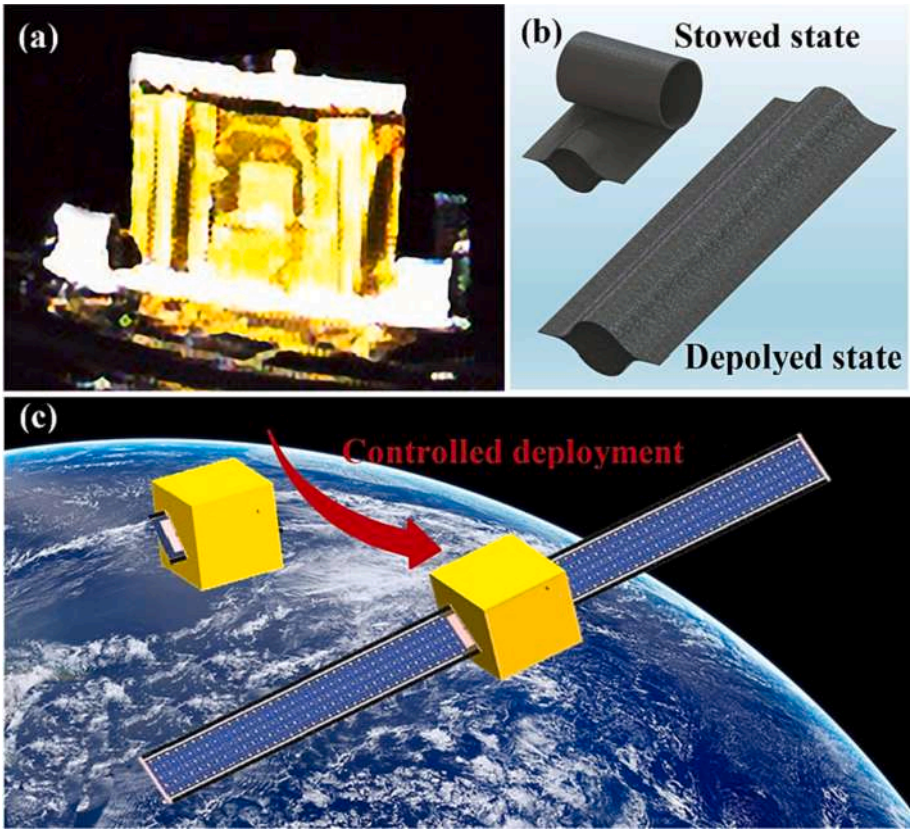

Fig. 11. Flexible solar array systems based on SMPCs lenticular tube: (a) on orbit demonstrate; (b) lenticular tube based on SMPCs; (c) Concept application of future super large flexible solar array system based on SMPCs.

calculated, and then the analytical expressions of the key parameters under different damage systems were solved using the minimum energy principle. Key parameters include neutral surface position, critical buckling position, critical damage position, half-wavelength, and amplitude. Subsequently, the expressions and evolution rules of the bending moment, the equivalent bending stiffness, and the damage variable during the damage propagation process were obtained. Finally, the correctness of the theoretical analysis was verified by the bending test. Notably, the theoretical results of this study have been applied to design an SMPC-based lenticular tube. In the future, this study will serve for the design and optimization of super-large SMPC-based deployable structures.

Declaration of Competing Interest

The authors declare that they have no known competing financial interests or personal relationships that could have appeared to influence the work reported in this paper.

Data availability

Data will be made available on request.

Acknowledgements

The authors would like to thank the Heilongjiang Touyan Innovation Team Program. This work is supported by the National Natural Science Foundation of China (Grant No. 11632005, 11872020).

References

[1] Roth PJ, Lowe AB. Stimulus-responsive polymers. Polym Chem 2017;8(1):10–1.
[2] Liu T, Zhou T, Yao Y, Zhang F, Liu L, Liu Y, et al. Stimulus methods of multi-functional shape memory polymer nanocomposites: A review. Compos Part A Appl Sci Manuf 2017;100:20–30.
[3] Segiet D, Raidt T, Özdem H, Weckes S, Tiller JC, Katzenberg F. Thermo-/moisture-responsive shape-memory effect of poly (2-ethyl-2-oxazoline) networks. J Polym Sci, Part B: Polym Phys 2019;57(16):1053–61.
[4] Li A, Challapalli A, Li G. 4D printing of recyclable lightweight architectures using high recovery stress shape memory polymer. Sci Rep 2019;9(1):1–13.
[5] Luo L, Zhang F, Leng J. Shape memory epoxy resin and its composites: from materials to applications. Research 2022;2022:1–25.
[6] Herath M, Epaarachchi J, Islam M, Fang L, Leng J. Light activated shape memory polymers and composites: A review. Eur Polym J 2020;136:109912.
[7] Yoon J. Design-to-fabrication with thermo-responsive shape memory polymer applications for building skins. Archit Sci Rev 2021;64(1-2):72–86.
[8] Kim Y-J, Matsunaga YT. Thermo-responsive polymers and their application as smart biomaterials. J Mater Chem B 2017;5(23):4307–21.
[9] Meng H, Li G. A review of stimuli-responsive shape memory polymer composites. Polymer 2013;54(9):2199–221.
[10] McClung AJ, Tandon GP, Baur JW. Deformation rate-, hold time-, and cycle-dependent shape-memory performance of Veriflex-E resin. Mech Time-Depend Mat 2013;17(1):39–52.
[11] McClung AJ, Tandon GP, Baur JW. Strain rate-and temperature-dependent tensile properties of an epoxy-based, thermosetting, shape memory polymer (Veriflex-E). Mech Time-Depend Mat 2012;16(2):205–21.
[12] Guan X, Chen H, Xia H, Fu Y, Yao J, Ni Q-Q. Flexible energy harvester based on aligned PZT/SMPU nanofibers and shape memory effect for curved sensors. Compos Part B-Eng 2020;197:108169.
[13] Luo L, Zhang F, Leng J. Multi-performance shape memory epoxy resins and their composites with narrow transition temperature range. Compos Sci Technol 2021;213:108899.
[14] Roh J-H, Kim H-I, Lee S-Y. Viscoelastic effect on unfolding behaviors of shape memory composite booms. Compos Struct 2015;133:235–45.
[15] Tao R, Liu X, Yang QS, He XQ. Design and analysis of smart diaphragm based on shape memory polymer. J Appl Polym Sci 2018;135(31):46557.
[16] Meng Q, Hu J. A review of shape memory polymer composites and blends. Compos Part A Appl Sci Manuf 2009;40(11):1661–72.
[17] Liu T, Liu L, Yu M, Li Q, Zeng C, Lan X, et al. Integrative hinge based on shape memory polymer composites: Material, design, properties and application. Compos Struct 2018;206:164–76.
[18] Wang X, Lu H, Shi X, Yu K, Fu YQ. A thermomechanical model of multi-shape memory effect for amorphous polymer with tunable segment compositions. Compos Part B-Eng 2019;160:298–305.
[19] Wang X, Xu X, Zhou Z, Gou J. Shape memory polymer composite coatings with enhanced mechanical and antimicrobial properties. Pigm Resin Technol 2018;47(1):63–71.
[20] Andrianov IV, Kalamkarov AL, Weichert D. Buckling of fibers in fiber-reinforced composites. Compos Part B-Eng 2012;43(4):2058–62.
[21] Abrahamson ER, Lake MS, Munshi NA, Gall K. Shape Memory Mechanics of an Elastic Memory Composite Resin. J Intell Mater Syst Struct 2016;14(10):623–32.
[22] Liu Z, Li Q, Bian W, Lan X, Liu Y, Leng J. Preliminary test and analysis of an ultralight lenticular tube based on shape memory polymer composites. Compos Struct 2019;223:110936.
[23] Santo L, Bellisario D, Iorio L, Quadrini F. Shape memory composite structures for self-deployable solar sails. Astrodynamics 2019;3(3):247–55.
[24] Herath M, Epaarachchi J. Shape memory polymer composites and their smart structural applications. Compos Mater 2021:581–610.
[25] Campbell D, Maji A. Deployment accuracy and mechanics of elastic memory composites. In: Proceedings of 44th AIAA/ASME/ASCE/AHS/ASC Structures, Structural Dynamics, and Materials Conference. 2003.
[26] Campbell D, Mallick K, Lake M. A study of the compession mechanics of soft-resin composites. In: Proceedings of 45th AIAA/ASME/ASCE/AHS/ASC Structures, Structural Dynamics & Materials Conference. 2004.
[27] Lan X, Liu L, Liu Y, Leng J, Du S. Post microbuckling mechanics of fibre-reinforced shape-memory polymers undergoing flexure deformation. Mech Mater 2014;72:46–60.
[28] Lan X, Liu Y, Lv H, Wang X, Leng J, Du S. Fiber reinforced shape-memory polymer composite and its application in a deployable hinge. Smart Mater Struct 2009;18(2):024002.
[29] Xiong ZY, Wang ZD, Li ZF, Chang RN. Micromechanism of deformation in EMC laminates. Mater Sci Eng A 2008;496(1–2):323–8.
[30] Zhang J, Dui G, Liang X. Revisiting the micro-buckling of carbon fibers in elastic memory composite plates under pure bending. Int J Mech Sci 2018;136:339–48.
[31] Xiong Z, Jin D, Yang Y, Zeng D. A theoretical investigation into the orientation of buckling direction of the reinforcing fibers in EMC laminate. Journal of Wuhan University of Technology-Mater Sci Ed 2014;29(1):148–53.
[32] Gall K, Mikulas M, Tupper M, Munshi N. Micro-mechanisms of deformation in fiber reinforced polymer matrix elastic memory composites. In: Proceedings of 19th AIAA Applied Aerodynamics Conference. 2001.
[33] Jones RM. Mechanics of composite materials. CRC Press 1998.
[34] Kelly A, Davies GJ. The principles of the fibre reinforcement of metals. Meta Rev 1965;10(1):1–77.
[35] Francis W, Lake M, Schultz M, Campbell D, Dunn M, Qi HJ. Elastic memory composite microbuckling mechanics: closed-form model with empirical correlation. In: Proceedings of 48th AIAA/ASME/ASCE/AHS/ASC Structures, Structural Dynamics, and Materials Conference. 2007.
[36] Lan X, Liu LiWu, Zhang FengHua, Liu ZhengXian, Wang LinLin, Li QiFeng, et al. World's first spaceflight on-orbit demonstration of a flexible solar array system based on shape memory polymer composites. Sci China Tech Sci 2020;63(8):1436–51.